SCIENCE CHINA
Earth Sciences

• RESEARCH PAPER •

June 2014 Vol.57 No.6: 1267–1277
doi: 10.1007/s11430-013-4796-x

Detection of crevasses over polar ice shelves using Satellite Laser Altimeter

LIU Yan[1,2], CHENG Xiao[1,2*], HUI FengMing[1,2], WANG XianWei[1,2], WANG Fang[1,2] & CHENG Cheng[2,3]

[1] *State Key Laboratory of Remote Sensing Science, Jointly Sponsored by Beijing Normal University and Institute of Remote Sensing and Digital Earth, Chinese Academy of Sciences, Beijing 100875, China;*
[2] *College of Global Change and Earth System Science, Beijing Normal University, Beijing 100875, China;*
[3] *School of Surveying and Urban Spatial Information Science, Beijing University of Civil Engineering and Architecture, Beijing 100044, China*

Received March 18, 2013; accepted June 20, 2013; published online February 19, 2014

Ice shelf breakups account for most mass loss from the Antarctic Ice Sheet as the consequence of the propagation of crevasses (or rift) in response to stress. Thus there is a pressing need for detecting crevasses' location and depth, to understand the mechanism of calving processes. This paper presents a method of crevasse detection using the ICESat-1/GLAS data. A case study was taken at the Amery Ice Shelf of Antarctica to verify the accuracy of geo-location and depth of crevasses detected. Moreover, based on the limited crevasse points, we developed a method to detect the peak stress points which can be used to track the location of the crack tips and to identify the possible high-risk area where an ice shelf begins to break up. The spatial and temporal distribution of crevasse depth and the spatial distribution of peak stress points of the Amery Ice Shelf were analyzed through 132 tracks in 16 campaign periods of ICESat-1/GLAS between 2003 and 2008. The results showed that the depth of the detected crevasse points ranged from 2 to 31.7 m, which were above the sea level; the crevasse that advected downstream to the front edge of an ice shelf has little possibility to directly result in breakups because the crevasse depth did not show any increasing trend over time; the local stress concentration is distributed mainly in the suture zones on the ice shelves.

satellite laser altimeter, ICESat-1/GLAS, crevasse, depth detection, ice shelves

Citation: Liu Y, Cheng X, Hui F M, et al. 2014. Detection of crevasses over polar ice shelves using Satellite Laser Altimeter. Science China: Earth Sciences, 57: 1267−1277, doi: 10.1007/s11430-013-4796-x

Iceberg calving is an important component of the mass balance of the Antarctic ice-sheet, and it accounts for most of the mass loss of the Antarctic ice-sheets (Jacobs et al., 1992; Rignot et al., 2008). Understanding the mechanism underlying calving is key to accurately predicting the response of the cryosphere to future climate forces and sea level changes. However, only a few ice-sheet models have attempted to represent calving mechanism, although it has been the focus of a great deal of current research. Calving can be regarded as a result of propagation of stress-induced crevassing. The position, scale, and duration of ice shelf calving are heavily influenced by the location, distribution, orientation, and propagation features of crevasses at the front edge of the ice shelf (Benn et al., 2007). The propagation features of a given crevasse are the spatial and temporal variations of its horizontal length and vertical depth. For this reason, detecting the positions and depths of ice crevasses is critical to studying the rule of crevassing propagation, to understanding the calving mechanism, and to predicting calving.

Crevasse detection includes field surveys and remote

*Corresponding author (email: xcheng@bnu.edu.cn)

sensing studies. Field surveys measure the positions and depths of crevasses, typically by identifying discontinuities in the firn layer using Ground penetrating radar (GPR) image, high-amplitude reflections from the snow bridges covering the crevasses, and hyperbolic diffractions from the nearly vertical side walls (Delaney et al., 2004; Koh et al., 2010; Mercer et al., 2010; Taurisano et al., 2006; Zamora et al., 2007). These field works are mainly used for polar exploration and observation, allowing explorers to avoid the danger posed by crevasses along the travel route. Remote sensing detection uses optical or radar sensors on aircrafts or satellites to image distinctive features in the surficial geometry patterns of crevasses, which allows researchers to collect surface geometry information, such as the positions, distribution, and orientations of the crevasses (Glasser et al., 2009; Vornberger et al., 1990; Xu et al., 2011). This technique was originally applied to the study of the movement physics and disintegration processes of ice flows, including inversion of their movement history (MacAyeal et al., 1988) and velocity gradients (Vornberger et al., 1990), derivation of their stress fields, and fracture laws (Harper et al., 1998; Vaughan, 1993). In recent years, analyses have been combined with simulations based on the features of ice shelf crevasses and other glacier properties such as those of melt pools on the ice surface. These combined studies have indicated that surficial melt water in summer seasons flowed into pre-existing crevasses in ice shelves, causing the catastrophic collapse of the Larsen (A and B) and Wilkins ice shelves in the Antarctic Peninsula (Glasser et al., 2008; Scambos et al., 2009; Scambos et al., 2003). However, passive remote sensed optical and radar imaging cannot measure vertical distances (depth) but only provide surficial geometric features of crevasses. Currently available disintegration models usually employ surficial strain rates to determine crevasse depths, but few of these models have been validated by observation data (Mottram et al., 2009).

Geoscience Laser Altimeter System (GLAS) instrument on the U.S. Ice, Cloud, and Land Elevation Satellite (ICESat-1) can measure elevation down to the centimeter level (Shuman et al., 2006). Taking advantage of the V-shape elevation profile characteristics of crevasses revealed by the ICESat-1 elevation footprints, here we propose a new method for detecting crevasse positions and measuring crevasse depths. We use the Amery Ice Shelf in Antarctica to assess this method. Through analyzing the spatial and temporal distribution of depth values of detection points, we extracted information useful for understanding crevasse formation and ice shelf disintegration.

1 Study area and datasets

The Amery Ice Shelf is the largest ice shelf in the East Antarctica, where the ground ice of the Lambert, Mellor and Fisher and other Glaciers drain, with the length of 550 km from 73°S to 68.5°S (Fricker et al., 2002). Its width ranges from 40 km near the grounding line to 200 km at the ice-shelf front, and its velocities vary from 300 to 1350 m/yr (Young et al., 2002) Since all ice is discharged through a narrow outlet of about 200 km, the ice shelf system is very active and extremely sensitive to the change of global climate and sea-level rise.

The ice textural features on the Amery Ice Shelf mainly include the ice-shelf front, crevasses, rifts and longitudinal linear surface structures (Figure 1). Longitudinal linear surface structures characterize the ice flow, including "suture zone" between different ice flow bands. Suture zone is usually about 1.5 km wide with the local subsidence terrain (Fricker et al., 2009), and extends from the grounding line to the ice shelf front. The collapse of ice shelf may be caused by partial rupturing of the suture zones (Glasser et al., 2008). The ice front rift is different from crevasse in that the former penetrates the entire ice shelf thickness whereas the latter does not. There are three large rifts, Rift L1, L2, and L3, at the front of the Amery Ice Shelf. The Rift L1 generated two new rifts, Rift T1 and T2, which are known as the "Loose Tooth" of the Amery Ice Shelf (Fricker et al., 2005). The Amery Ice Shelf has two significant crevasse swarms, Swarm A and B (Hambrey et al., 1994), with the length between 10 and 50 km and the width between 500 and 1200 m. Swarm A extends from the Thil Island to the ice shelf front, and is about 150 km long and 10–50 km wide. The crevasse spacing ranges from 1 to 10 km. When the crevasse located at the position of the initial occurrence is moving downward along the ice flow direction, the crevasse tips extend inward toward the center line, ranging from a few miles to over 50 km. The crevasses are almost parallel to each other. The angle between the crevasse and the flow direction changes from about 45° at the initial to about 135° at the ice-shelf front. These crevasses give rise to new crevasses in the process of moving and these new crevasses are initially at an angle of about 45° with the flow direction. Swarm B extends from the Trost Rocks to the ice shelf front and consists of two sets of parallel moving crevasse bands. The crevasse swarm is very intensive, about 200 km long and 25–30 km wide. Swarm A and B are transverse crevasses according to their location, direction and velocity field. The transverse crevasse is the major crevasse type of the Antarctic ice shelves, which are caused by longitudinal tensile stress due to the difference of the lateral velocities. If we assume that the ice shelf is in stable situation with the constant velocity, it would require approximately 200 years for the crevasses to move from the initial point to the ice shelf front.

ICESat-1 is the first LiDAR satellite launched by the U.S. National Aeronautics and Space Administration (NASA) and GLAS is the first satellite laser radar sensor payload on this satellite platform. The major scientific mission of ICESat-1/GLAS is to measure ice sheet topography and its temporal variation, the characteristics of the clouds and the

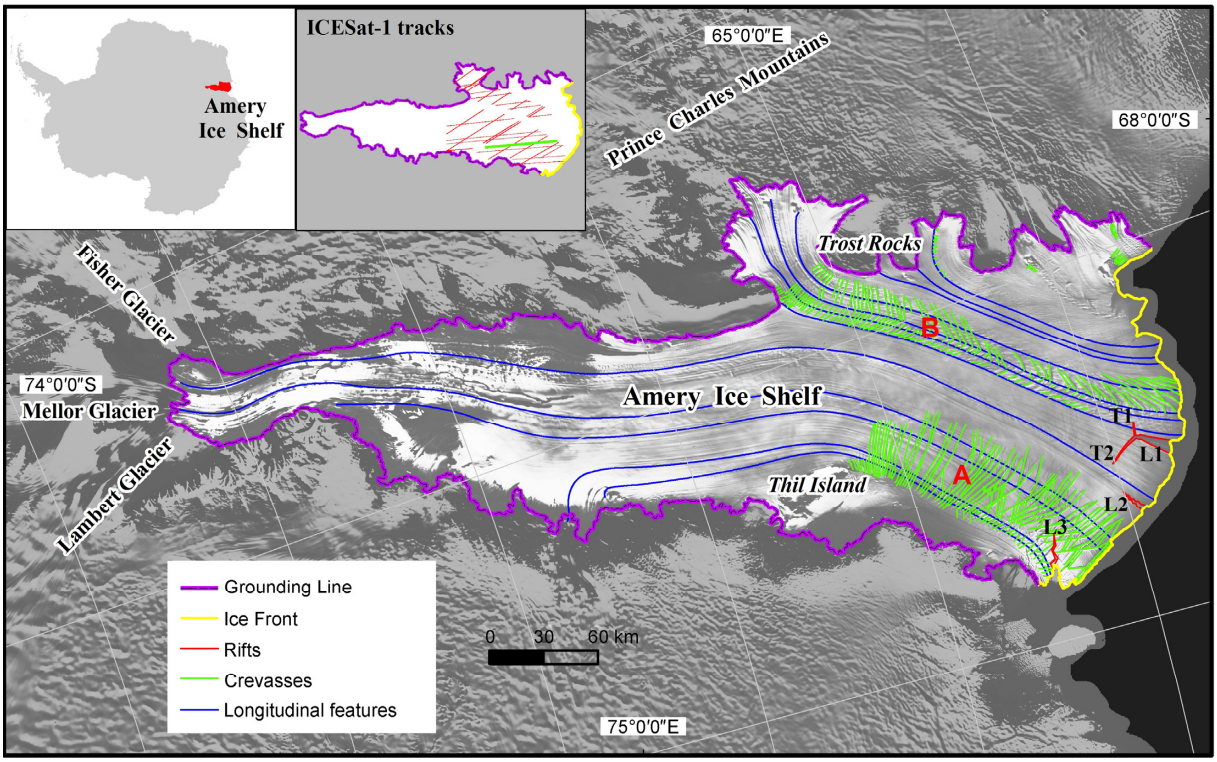

Figure 1 Sketch map of the characterized Amery Ice Shelf overlaid on MOA image. The green trajectory lines among the ICESat-1 tracks are the analytical sections of Figures 2–5.

atmosphere, the polar ice-sheet mass balance, and to understand how the Earth's atmosphere and climate change is affecting the polar ice-sheet mass balance and global sea level changes (E et al., 2009; Wang et al., 2011; Wang et al., 2012). The vertical accuracy of ICESat-1/GLAS satellite altimetry data is ±13.8 cm (Table 1), and the geo-location accuracy is better than 20 cm. The laser beam produces a series of approximately 70 m diameter spots (Shuman et al., 2006). This study used the ICESat-1/GLAS Antarctic and Greenland Ice Sheet Altimetry Data product GLA12 from 2003 to 2008, including 132 lines of 25 tracks in 16 campaign periods (Figure 1). The data cover the area of Swarm A and B and the repeated trajectory line of a track is up to seven. The data are shown in Table 2.

Other auxiliary data for validation and analysis of the results include the Band 2 images of Moderate-resolution Imaging Spectroradiometer (MODIS) covering the Amery Ice Shelf from 2003 to 2008 with the spatial resolution of

Table 1 IceSat-1/GLAS single-shot error budget for elevation measurements (Zwally et al., 2002)

Error source	Error (cm)
Precision orbit determination	±5
Precision attitude determination	±7.5
Atmospheric delay	±2
Atmospheric forward scattering	±2
Other errors such as tide	±1
Total error	±13.8

Table 2 ICESat-1/GLAS tracks covering the Amery Ice Shelf from 2003 to 2008

Ops period	Date	Number of tracks
L1A	2003-02-20–2003-03-21	7
L2A	2003-10-04–2003-11-19	2
L2A	2003-09-25–2003-10-04	15
L2B	2004-02-17–2004-03-21	9
L2C	2004-05-18–2004-06-21	8
L2D	2008-11-25–2008-12-17	1
L3A	2004-10-03–2004-11-08	9
L3B	2005-02-17–2005-03-24	4
L3C	2005-05-20–2005-06-23	13
L3D	2005-10-21–2005-11-24	9
L3E	2006-02-22–2006-03-28	5
L3G	2006-10-25–2006-11-27	21
L3H	2007-03-12–2007-04-14	10
L3I	2007-10-02–2007-11-05	11
L3J	2008-02-17–2008-03-21	4
L3K	2008-10-04–2008-10-19	4
Total	2003-02-20–2008-10-19	132

250 m, the grounding line products, and the mosaic products. MODIS images with geo-location accuracy less than one pixel (250 m) are used to validate the detected crevasses point. MODIS-based Mosaic of Antarctica (MOA) map was composed by 260 swaths of MODIS images acquired during the 2000–2004 austral summer (Scambos et al., 2007), which can be used to extract ice shelf surface texture characteristics such as suture zone. The data were downloaded from the U.S. National Snow and Ice Center (NSIDC) (http://nsidc.org/).

2 Methods

2.1 Crevasse detection and depth calculation

According to the V-shaped elevation profile of an ICESat-1/GLAS trajectory line (Figure 2), the crevasse positions and crevasse depth were obtained. The process is as follows:

(1) The basis of Crevasse detection. The elevation profile of a GLAS track line crossing the crevasses shows a relatively rapid decline and rise as a V-shaped profile (Figure 2). The V-shaped profile is on the crevasses (black and white stripes) shown on MODIS image at similar time phases, and its lowest point is corresponding to the position of alternating black and white (Figure 3). The V-shaped elevation profiles within a short distance were used to detect crevasses. Fricker et al. (2009) used the similar V-shaped profile characteristics of ICESat-1/GLAS track line to identify the elevation drop of suture zones at the southernmost part of the Amery Ice Shelf (Fricker et al., 2009). In fact, the elevation drops of crevasses are much larger than those of suture zones.

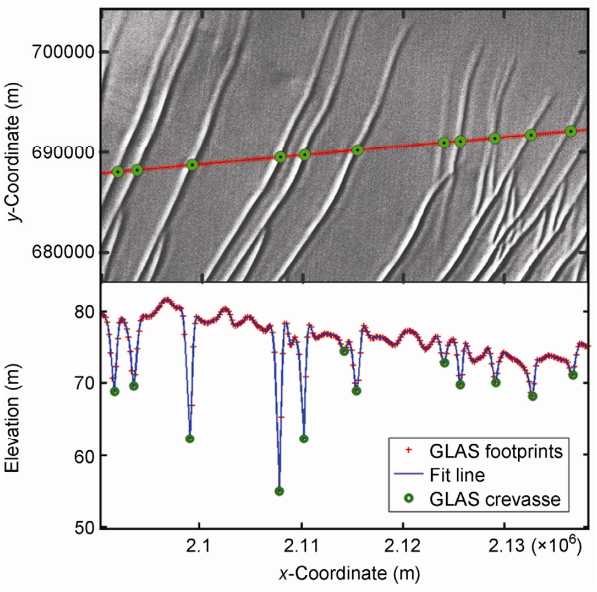

Figure 2 Elevation profile of GLAS footprints (L1A2003-2-26) overlaid on Landsat-7 ETM+ image on November 17, 2002.

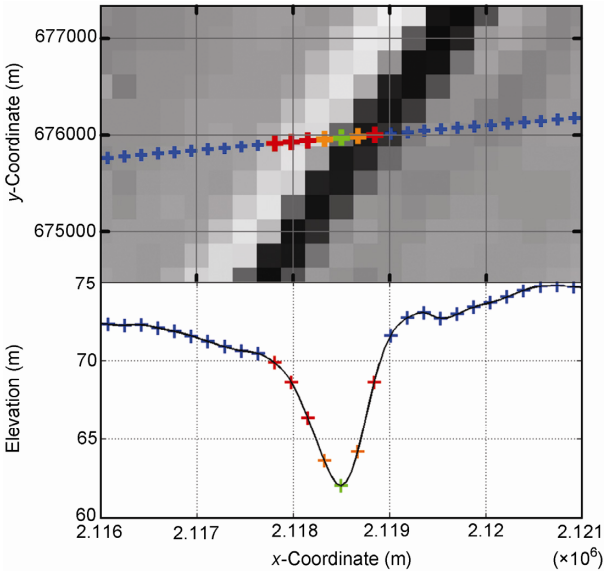

Figure 3 Elevation profile of GLAS footprints (L1A2004-10-20) overlaid on MODIS image on October 20, 2002.

(2) Crevasse position detection. The automatic detection process is as follows:

According to the width of the crevasses along the track direction, the number of continuous GLAS footprints of each detection unit is determined, which is smaller than the number of between two crevasses but greater than that falling into a single crevasse. Eight was selected in this paper. The track line is divided into m units, m=int(n/8), where n is the total number of footprints of the GLAS track line.

The highest elevation point and the lowest elevation point are obtained in each detection unit, and the elevation difference between them is calculated.

A threshold value for elevation difference is used to distinct the V-shaped profile of the crevasses from that of the suture zones or the ups and downs of the surface terrain. On the Amery Ice Shelf, the elevation difference threshold steps of 0.5, 1, 1.5, 2, and 2.5 m were tested to obtain the concave points. The detected lowest elevation points were validated by comparing with the MODIS image. The results showed that when the threshold is set as 1.5 m, there are many erroneous points; when the threshold is set as 2.5 m, many points would be ignored; while the threshold of 2 m can obtain better results. Therefore, the optimal threshold value is at 0.5 m step. This threshold selection method can be applied in other regions and the optimal threshold may be different.

According to the smallest elevation footprint in a detection unit, whether or not a V-shape profile is in this unit is determined by comparing this smallest elevation with that of the three footprints before and after that footprint. If this smallest elevation value is the minimum one, then this footprint is identified as the bottom footprint of the crevasse (Figure 2), which is also referred as GLAS crevasse point; otherwise, no V-shaped profile is in the detection unit.

(3) Crevasse depth calculation. Crevasse depth is the difference between the surface elevation and the elevation of the crevasse bottom.

To obtain the crevasse bottom elevation. The position of the GLAS crevasse point is not exactly the bottommost point of the crevasse. According to the crevassed section showing V-shaped characteristics, different interpolation method tests showed that the cubic spline interpolation method (De Boor 2001) has a good fit of the vertical cross-section of a crevasse (shown in Figure 4, black line), and GLAS footprints are all on the curve fitting profile. Therefore, the cubic spline interpolation method was used to fit the vertical profile of the crevasses. Although the position of the GLAS crevasse point is not exactly the crevasse bottom point, it is still the closest point to the bottom. To search the minimum value of the crevasse profile curve $x_{\min}$, $y_{\min}$ and their corresponding elevations $h_{x_{\min}}$, $h_{y_{\min}}$, in the x-direction and y-direction, respectively, ($x_{\min}$, $y_{\min}$) is the position of crevasse bottom and the mean value of $h_{x_{\min}}$ and $h_{y_{\min}}$ is the elevation of the crevasse bottom h_{bot}.

To obtain the surface elevation. The footprints between the maximum elevation footprint of eight footprints before the GLAS crevasse point and that after the GLAS crevasse is set as the points related to the crevasse. Removing these footprints, cubic spline interpolation method with the rest footprints is used to fit ice shelf surface profile (red line shown in Figure 4). To calculate the ice surface elevation $h_{tx_{\min}}$, $h_{ty_{\min}}$ at crevasses bottommost position $x_{\min}$, $y_{\min}$ and h_{top} is the mean value of $h_{tx_{\min}}$ and $h_{ty_{\min}}$. The crevasse depth is calculated as:

$$Depth = h_{\text{top}} - h_{\text{bot}}. \quad (1)$$

(4) Depth threshold. On the Amery Ice Shelf, the depth difference threshold steps of 1.9, 2.0, and 2.1 m were tested to obtain the optimal threshold. The result showed 2.0 m is an optimal choice (still a small amount of missing points). This threshold selection method can be applied in other regions and the optimal threshold may be different.

2.2 Detection of crevasses peak stress point

Crevasse formation and crevasse depth modeling are based mainly on the theory of linear elastic fracture mechanics (LEFM). It is assumed that all materials including small size fracture or gap (centimeter-level) are distributed in the local stress concentration in the description of the initial rupture location and crack propagation principles of brittle materials. When the stress intensity factor reaches the threshold value, these "initial rips" begin to spread and form fractures (Nath et al., 2003). In other words, local stress concentration is a necessary condition of the crevasse formation. Local stress field always has a peak stress (the maximum stress point), thus the detection of the crevasse peak stress point is one way to explore the location of "initial rip". In addition, local stress concentration is also regarded as a fragile area of ice shelves, which easily leads to the formation of crevasse and ice shelf break-up at the ice front. Therefore, the detection of the peak stress points has significance on the crevasse propagation and calving modeling of ice shelves.

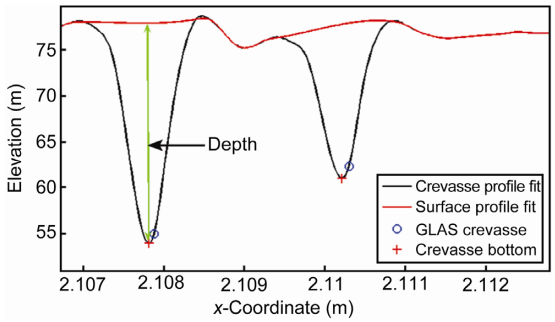

Figure 4 Sketch map of crevasse depth calculation.

The peak stress point is detected based on the feature of the Λ-shape crevasse depth profile along the GLAS track.

(1) Theoretical basis of the detection of the crevasse peak stress point. The stress distribution of local stress concentration has the characteristic that the stress decreases rapidly with the increase of the spacing with the peak stress point, that is, the stress profile of the local stress concentration field will show a Λ-shape structure. According to Nye (1955)'s rule for crevasse depth propagation, the formula of the crevasse depth in area of the crevasse swarm is as follows:

$$Depth = T/\rho_{\text{ice}}g, \quad (2)$$

where T denotes the average tensile stress, ρ_{ice} is the ice density, and g is the gravitational acceleration (Weertman 1973). Eq. (2) ignores the effect of the stress concentration of crevasse tip, suitable for closely spaced crevasses. The assumption of a proportional relationship between tensile stress and the crevasse depth is commonly considered as the basis of crevasse formation and propagation models (Rist et al., 1999; Van der Veen, 1999). Based on this assumption, the distribution of the crevasse depth should be consistent with the stress distribution. The Λ-shape structure (Figure 5) was found on the crevasse depth profile along the GLAS track. i.e., the rapid depth changes within a short distance, which fits the characteristics of local stress concentration. As shown in Figure 5, there are two distinct depth peaks of the two different trajectory lines along the same track. The GLAS footprints may not be able to precisely detect the locations of the crevasse depth peak points, but the detected peak points should be very close to the local crevasse depth peak points. Therefore, the crevasses peak stress point is detected through the detection of the crevasse depth peak point.

(2) Recognition of the crevassed peak stress point. Crevasse peak stress point should be the point with the maximum crevasse depth among the different trajectory lines along the

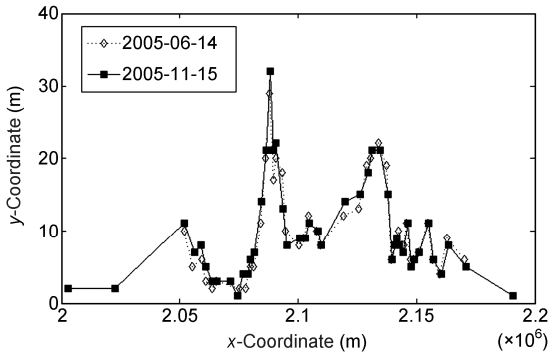

Figure 5 Crevasse depth profile along a track.

same track. The depth difference between the local maximum point and the minimum point is required to be greater than 5 m in this paper. As it is impossible to detect a complete depth profile of a crevasse, the location of the detected peak stress is the approximate location of the true peak stress point.

2.3 Analysis method of crevasse depth variation

Crevasse depth variation analysis is designed to understand the characteristics of the crevasse propagation, including temporal variation of the crevasse depth, changes in the advection process to the ice shelf front (i.e., changes along the flow direction) as well as changes along crevasse propagation direction (i.e., changes along the vertical direction of ice flow). It is difficult to have an accurate assessment of the changes of crevasse depth because of the three factors: incomplete repeating covering of the GLAS trajectory point, sparse distribution of the crevasse points, and the movement of crevasses along the ice flow. Nevertheless, approximate strategy can make a rough assessment of the crevasse depth changes based on the distribution of the existing measurements.

Since the length of crevasses in Swath A is much longer and more crevasse points were detected by using GLAS data, the measurements in Swath A were used to the variation analysis of crevasse depth.

(1) The strategy of choosing the approximate crevasse points with small distance between them was used to undercut the impact of spatial depth variation in the analysis of the temporal depth variation. This paper used a relatively uniform distribution of 158 approximate crevasse point pairs with relatively mutual distance less than 1 km (time span from 2003 to 2007). *T*-test method was used to validate the assumption that the approximate crevasse point pairs with little spatial variation, i.e., the probability density distribution of the depth difference between the approximate crevasse pairs obeys the assumption of a normal distribution with mean 0 (p=0.85).

(2) The spatial average strategies were employed to undercut the impact of the temporal depth variation for the analysis of the crevasse depth changes along the ice flow direction and the vertical direction of ice flow. The crevasse swarm, about 112 km long and 45 km wide, was divided into a grid net of 32 (row) by 18 (column) (Figure 6). The results show the average number of the crevasse points falling into a row is 21.9 and 39.9 falling into a column. The minimum time span is more than two years. Two methods were used to undercut the influences of the temporal variation of the depth and the mutual influence in the two directions.

The depth variations along the ice flow and across the ice flow were assessed directly from the statistics of the average value of crevasse depths in each column or row.

The ice flow direction was considered as the x-axis and the vertical direction of ice flow as the y-axis. In this coordinate system, the depth of each grid cell is obtained by Kriging interpolation method using the depths of grid cells that have crevasse depth measurements (Figure 6). Then, the depth variations along the ice flow and across the ice flow were assessed from the statistics of the interpolation data.

3 Results

3.1 Results of crevasse detection and accuracy verification

Figure 7 shows the spatial distribution of crevasse depths based on GLAS footprints collected on the Amery Ice Shelf from 2003 to 2008. In general, crevasses are relatively shallow at both tapering tips. The distribution of these depths showed no monotonic tendency to either increase or decrease along the direction either parallel or normal to the ice flow. However, the depth was found to locally decrease at both sides of some maxima points. A total of 1269 crevasse points were detected on the Amery Ice Shelf, which had an average depth of 8.15 m. Swarm A had 950 detection points with an average depth of 8.9 m. Swarm B had 319 points, which had an average depth of 6.0 m. There were only two crevasse points whose depths exceeded 30 m. The greatest depth (37.1 m) was recorded in Rift L3 in Swarm A. This

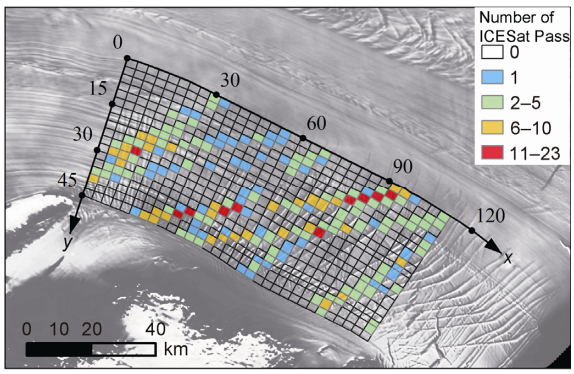

Figure 6 Grid distribution of Swarm A overlaid on MOA image.

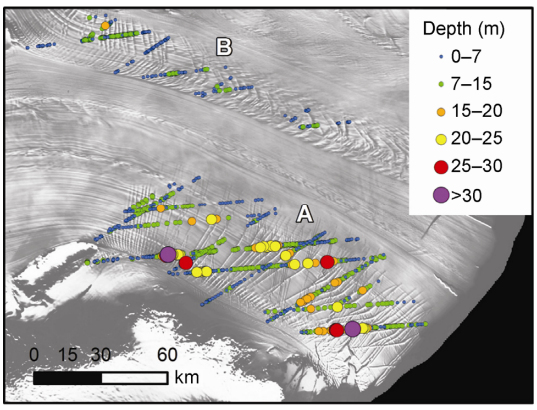

Figure 7 Spatial distributions of GLAS crevasse depths of the Amery Ice Shelf from 2003 to 2008 overlaid on MOA image.

depth value was measured from the snow-ice mixture at the crevasse bottom to its ice surface. The other one (a depth of 31.7 m) was located near one side edge of the ice shelf about 70 km from the front edge. The point found in Rift L3 was considered outliers and excluded from crevasses. The crevasse depth ranged from 2.0 to 31.7 m.

The crevasse points extracted from the ICESat-1/GLAS data were compared to MODIS images taken at about the similar time phase, validating the accuracy of the position detection method. Two sets of data collected at about the same time phase and adjacent positions were used to assess the precision of our depth measurement method.

As shown in Figure 8, every point in every crevasse detected in 2004 was consistent with crevasse data collected using the MODIS images on September 4, 2004. (All data were collected no more than 7 months apart.) In addition, most of the points that were shallower than 2 m fell inside the suture zone of the ice shelf.

Because of the dearth of physically measured depth data, this work employed a cross-validation method to examine the precision of our depth detection results. We selected two sets of depth data for the same crevasse group detected at about the same time phase at adjacent positions. We considered the first set to be true values of depth and the second to be measured ones. Each was used to evaluate the precision of our results. For example, the GLAS data collected on February 20, 2003 and October 20, 2004 were cross verified with their counterparts collected on March 8, 2003 and October 28, 2004, respectively (Figure 9). These two sets contained a total of 46 samples, collected no more than 16 days apart and from space no more than 267 m apart. The average depth of these crevasse points was 10.1 m. As shown in Table 3, the correlation coefficient (R^2) between the crevasse depths of the two sets was as high as 0.994, and the average error was only –0.02 m with a standard deviation of ±0.45 m.

3.2 Distribution characteristics of peak stress points

Figure 10 shows 26 crevasse points with quasi-peak stresses. These were detected along 12 GLAS orbits passing Swarm A. These crevasse points had depths ranging from 7.2 to 37.3 m, including points falling inside the crevasses. As shown in the figure, almost all the peak stress points are located inside the suture zone of the ice flow or adjacent areas, but none were at the tips of the crevasses. Within regions intersecting primary crevasses by an angle close to or greater than 90°, new crevasses formed near these peak stress points (The time of the crevasse formation was inferred from the angle between the new crevasse and the direction of the ice flow, which was close to 45°). Twenty-one of these peak stress points abutted the suture zones of four different ice flows, distributed down the directions of the flows. However, there was no monotonic variation in the depths of these peak stress points down the directions of the ice flows.

Figure 11 shows the spatial distribution of averaged crevasse depths along directions both parallel and normal to the ice flow in area A of the Amery Ice Shelf. As shown in Figure 11(a), the crevasse depths varied down the direction of the ice flow and showed no monotonically varying trend. As shown in Figure 11(b), there were two evident peak values

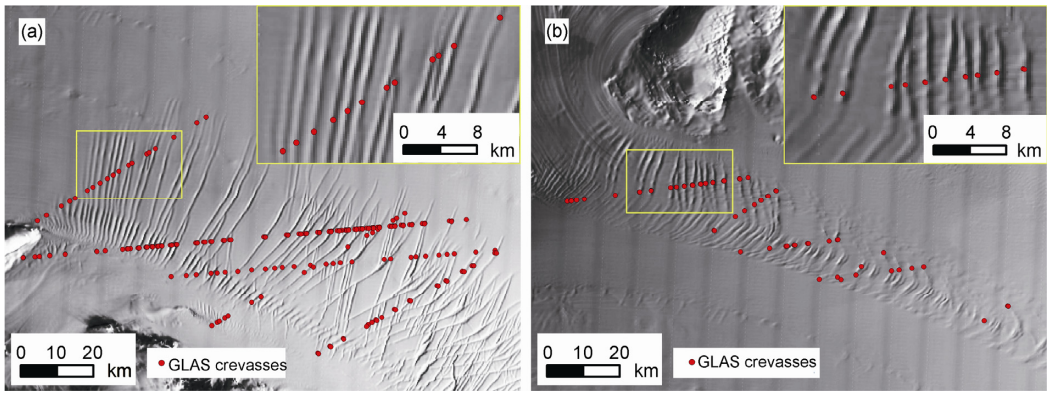

Figure 8 Crevasse detected in 2004 overlaid on MODIS image on September 4, 2004.

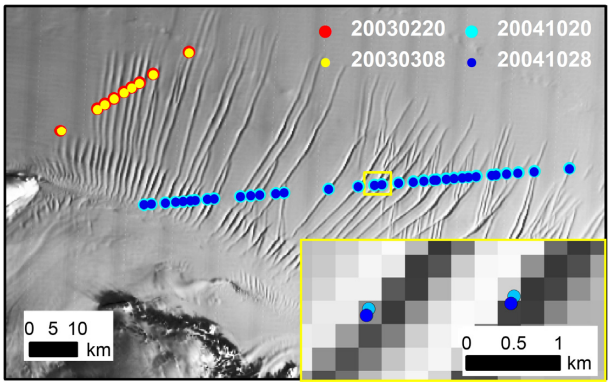

Figure 9 Distribution of the two set crevasses overlaid on MODIS image on September 4, 2004.

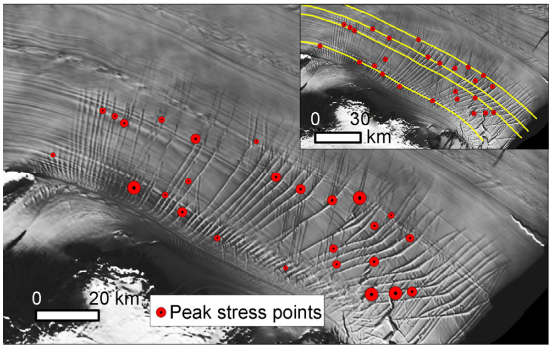

Figure 10 Distribution of crevasse peak stress points in Swarm A overlaid on MOA image; the yellow lines in the upper right corner are signed for suture zones.

Table 3 Results of cross-validation

Date	The first set 2004-10-20 2004-10-28	The second set 2003-2-20 2003-3-8	Total
Number of point pairs	37	9	46
Date difference	8	16	16
Maximum distance (m)	266.4	232.6	266.4
Correlation coefficient (R^2)	0.994	0.995	0.994
Mean error (m)	–0.05	0.15	–0.02
Standard deviation (m)	±0.49	±0.30	±0.45

in the averaged crevasse depth along the direction normal to the ice flow. The two peaks were separated by about 25 km. The regions in which the depth peaks were found corresponded to the peak stress points of the crevasse.

3.3 Temporal and Spatial distribution of crevasse depth

Table 4 shows annual changes in the crevasse depths over a four-year period. Slight differences were seen, all far less profound than annual variations.

Table 4 Annual changes in the crevasse depth from 2003 to 2007

	2003–2004	2004–2005	2005–2006	2006–2007
Number of point pairs	39	36	43	40
Average depth (m)	8.56	11.38	9.07	8.74
Average depth variation (m)	–0.06	0.03	–0.03	0.15
Standard deviation (m)	±1.34	±3.09	±2.31	±1.20

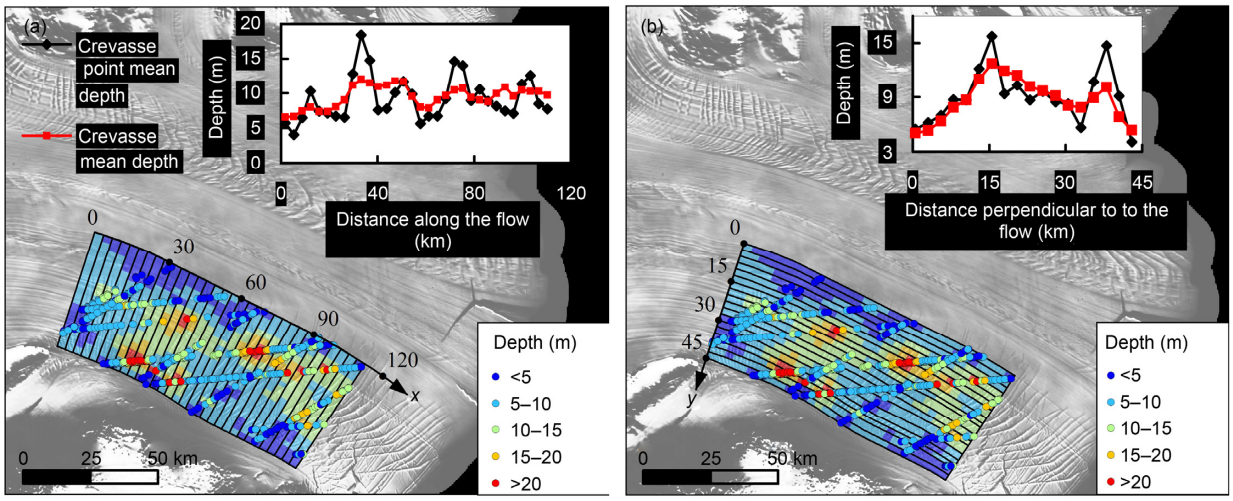

Figure 11 Distribution of crevasse depth overlaid on MOA image.

4 Discussions

For the Amery Ice Shelf, the elevation data detected by ICESat-1/GLAS showed 1269 crevasse points, with their depths ranging from 2.0 to 31.7 m. There is another detection point, which falls into Rift L3 at the front edge of the ice shelf. Its depth, 37.5 m, suggests that all the crevasses on the ice shelf were above sea level. By comparing these data to the relevant MODIS images at similar time phases, we found that the V-shape elevation profile based on ICESat-1/GLAS location could accurately indicate the position of a crevasse, and the cross validation facilitated high-precision depth detection. Although no suitable field measurement data were available for evaluating the absolute precision of the depth detection values, the cross-validation results generally showed that our method of depth detection was a reasonably accurate mean of assessing the differences in depth among crevasses. The crevasses in our working areas were relatively wide, and their depths showed no tendency to decrease over time. Similarly, the moving crevasses down the direction of the ice flow did not tend to decrease their depths over time (Upstream and downstream crevasses could form anywhere from tens to hundreds of years apart). This showed that the crevasse profile is little affected by snow cover and that the detected crevasse depths are probably close to their true values.

In this work, we proposed a method of detecting quasi-peak stress points in a crevasse based on the Λ-shape depth profile of the crevasse points. This method assumes a linear relationship between the tensile stress and the depth of a crevasse, as in previous studies (Rist et al., 1999; Van der Veen, 1999; Weertman, 1973). The method is supported by our observation of correspondence between the Λ-shape feature of the crevasse depth profile and the stress distribution at positions where local stresses are concentrated. The test on the Amery Ice Shelf indicates that peak stress points of a crevasse mostly occur within the suture zone of the ice shelf. Fricker et al. (2009) found the elevation of the suture zone to be markedly lower than that of surrounding ice surface, producing a groove normal to the ice flow (Fricker et al., 2009). This topography meets the surface geometry conditions to create local concentrations of stress. Moreover, new crevasses formed near those peak stress points of the primary crevasses in flowing motion. For these reasons, we believe that local stresses tend to concentrate within the suture zone of an ice flow, creating ice crevasses, which is even more incidental at the front edge of the shelf and so leads to disintegration of that ice shelf. Such inference strongly supports the previous assumptions that partial breakage of the suture zone is a requirement for ice shelf disintegration (Glasser et al., 2008) and that it renders the suture zone very fragile (Fricker et al., 2009). This contradicts the conclusion drawn by Huble et al. (2010) that the tapering tips of crevasses tend to occur in the suture zones (Hulbe et al., 2010). This conclusion was based on their analyses of the surface texture of the ice shelf and their simulations of the crevasses. In terms of the surface texture of the Amery Ice Shelf, our study did not find the trend of the crevasse tips to be enriched in the suture zone. We also noticed that the peak stress points of the crevasses were concentrated in only four suture zones, whereas some other distinct suture zones exhibited no peak stress points with local stress concentrations. In this way the presence of a suture zone is not a sufficient condition itself for local stress concentration. Other than the recognizable geometric distinctions in the surface texture obtained from remote sensing images, there must be other factors contributing to the local stress concentrations. As a result, detection of the depth of the crevasses is especially important in studies of the propagation of crevasse depth.

GLAS orbit data can be used to detect only a limited number of unevenly distributed crevasse points. Because ice flows are in continuous motion, this makes it difficult to distinguish between temporal and spatial variations in crevasse depth, and between lengthwise and down-flow variations. Nevertheless, some conclusions can still be drawn from the spatial and temporal distribution of the limited number of crevasse points. The annual variations in crevasse depth were very slight from 2003 to 2007. There was no trend of monotonic increase or decrease in the averaged crevasse depth in the regional unit down the ice flow direction, or in the depths of the peak stress points along the same ice flow line. These observations corroborated the inference that the depths of these crevasses generally do not increase over time and translational motion after the crevasses form. Because the depths of these crevasses are all below sea level, no disintegration would occur even if the crevasses move to the front edge of the ice shelf. This is consistent with the conclusion reached by Cook (2012)'s calving modeling that an ice crevasse moving to the front edge of a shelf cannot collapse unless it is filled with melt water (Cook et al., 2012).

Two evident peak values of the averaged crevasse depth were observed in the ice flow zonal unit along the direction extended lengthwise from the crevasse. These peak stress points fall right within the ice flow bands corresponding to these two peak values. This means that local stress concentrations occur not only during the formation of the primary crevasse but also during crevasse propagation, likely leading to creation of new secondary crevasses on the primary one. However, it also suggests that stress concentrations tend to arise in a relatively immobile ice flow zone. Accordingly, although crevasses undergoing translational motion probably cannot cause disintegration of the ice shelf, external forces at the front edge or crevasse propagation to the fragile ice flow zone may expedite crevasse depth propagation, leading to ice shelf break-up.

5 Conclusions

Here we propose a method of detecting surface crevasses in

an ice shelf using elevation data produced by ICESat-1/GLAS data. This method was tested on the Amery Ice Shelf and the results showed that the elevation data measured using a satellite laser could be used to extract precise information regarding the position and depth of the crevasses on the surfaces of the polar ice shelf. Accordingly, this method is considered an important complement to traditional passive remote sensing techniques for detecting ice crevasses. Although a complete crevasse depth profile cannot be detected due to limitation on the ICESat-1 orbit, we also suggest a method of detecting local stress concentrations in an ice shelf based on the depth distribution characteristics of a limited number of crevasse points. This method can be used to track the position of a primary crevasse and detect high-risk areas of ice shelf disintegration. The depth detection results from the Amery Ice Shelf indicate that the crevasses studied here had the following characteristics. (1) The crevasse depths are above sea level, and have very slight annual variations. No monotonic changes were detected either in crevasse depth down the ice flow direction, or in depth of peak stress points along the same ice flow line. These observations support the inference that the depth of a crevasse does not increase over time or translational motion once the crevasse forms. We therefore believe that crevasses that move to the front edge of an ice shelf cannot directly cause its disintegration. (2) The local stress concentrations of an ice shelf mostly occur within the suture zone of the ice flow, as suggested by the distribution of quasi-peak stress points and by the presence of two evident peak values in the direction normal to the ice flow.

The orbit limitation of ICESat-1/GLAS data and its ended mission make it impossible to perform densified and continual detections of ice crevasses. The ice-sheet detection satellite Cryosat-2, which was launched by the European Space Agency (ESA) in 2010, has a radar altimeter that renders it capable of detecting elevation as precisely as ICESat-1/GLAS. Because it has good penetrability, interference performance, and flexible orbit tuning, Cryosat-2 may facilitate crevasse analysis more precisely and with better coverage than ICESat-1, providing continual detection of the position and depth of crevasses.

This work was supported by the Chinese Arctic and Antarctic Administration, Fundamental Research Funds for the Central Universities (Grant No. 105560GK), National Basic Research Program of China (Grant No. 2012CB957704), National High-tech R&D Program of China (Grant Nos. 2008AA121702 and 2008AA09Z117), and National Natural Science Foundation of China (Grant Nos. 41176163 and 41106157). We are grateful to the National Snow and Ice Data Center (NSIDC) for providing GLA12 dataset of ICESat-1/GLAS and MODIS Mosaic of Antarctica (MOA) dataset. We thank the anonymous reviewers for their valuable comments and suggestions.

Benn D I, Warren C R, Mottram R H. 2007. Calving processes and the dynamics of calving glaciers. Earth-Sci Rev, 3-4: 143–179

Cook S, Zwinger T, Rutt I, et al. 2012. Testing the effect of water in crevasses on a physically based calving model. Ann Glaciol, 60: 90–96

De Boor C. 2001. A Practical Guide to Splines (revised ed.). New York: Springer

Delaney A J, Arcone S A, O'Bannon A, et al. 2004. Crevasse detection with GPR across the Ross Ice Shelf, Antarctica. 10th Interntionol Conferences on Ground Penetrating Radar, Delft, the Netherlands

E Dongchen, Sheng Q, Xu Y. 2009. High-accuracy topographical information extraction based on fusion of ASTER stereo-data and ICESat/GLAS data in Antarctica. Sci China Ser D-Earth Sci, 5: 714–722

Fricker H, Young N, Coleman R, et al. 2005. Multi-year monitoring of rift propagation on the Amery Ice Shelf, East Antarctica. Geophys Res Lett, 32: L02502

Fricker H A, Allison I, Craven M, et al. 2002. Redefinition of the Amery Ice Shelf, East Antarctica, grounding zone. J Geophys Res, 107: 2092–2096

Fricker H A, Coleman R, Padman L, et al. 2009. Mapping the grounding zone of the Amery Ice Shelf, East Antarctica using InSAR, MODIS and ICESat. Antarct Sci, 5: 515–532

Glasser N, Scambos T. 2008. A structural glaciological analysis of the 2002 Larsen B ice-shelf collapse. J Glaciol, 184: 3–16

Glasser N F, Kulessa B, Luckman A, et al. 2009. Surface structure and stability of the Larsen C ice shelf, Antarctic Peninsula. J Glaciol, 191: 400–410

Hambrey M J, Dowdeswell J A. 1994. Flow regime of the Lambert Glacier-Amery Ice Shelf system, Antarctica: Structural evidence from Landsat imagery. Ann Glaciol, 1: 401–406

Harper J, Humphrey I. 1998. Crevasse patterns and the strain-rate tensor: A high-resolution comparison. J Glaciol, 146: 68–76

Hulbe C L, LeDoux C, Cruikshank K. 2010. Propagation of long fractures in the Ronne Ice Shelf, Antarctica, investigated using a numerical model of fracture propagation. J Glaciol, 197: 459–472

Jacobs S S, Helmer H H, Doake C S M, et al. 1992. Melt of ice shelves and the mass balance of Antarctica. J Glaciol, 130: 375–387

Koh G, Lever J H, Arcone S A, et al. 2010 Autonomous FMCW radar survey of Antarctic shear zone. Ground Penetrating Radar (GPR), 2010 13th International Conference IEEE. 1–5

MacAyeal D, Bindschadler R, Jezek K, et al. 1988. Can relict crevasse plumes on Antarctic ice shelves reveal a history of ice-stream fluctuation. Ann Glaciol, 11: 77–82

Mercer J, Lever J, Newman S, et al. 2010 Crevasse Detection and Avoidance for Safe Traversing on the Dynamic and Annually Changing Margin of the Greenland Ice Sheet. American Geophysical Union, Fall Meeting 2010: abstract #C23B-0624

Mottram R H, Benn D I. 2009. Testing crevasse-depth models: A field study at Breiethamerkurjokull, Iceland. J Glaciol, 192: 746–752

Nath P, Vaughan D. 2003. Subsurface crevasse formation in glaciers and ice sheets. J Geophys Res, 108(B1): 2020, doi: 10.1029/2001JB000453

Rignot E, Bamber J L, Van den Broeke M R, et al. 2008. Recent Antarctic ice mass loss from radar interferometry and regional climate modelling. Nat Geosci, 2: 106–110

Rist M, Sammonds P, Murrell S, et al. 1999. Experimental and theoretical fracture mechanics applied to Antarctic ice fracture and surface crevassing. J Geophys Res, B2: 2973–2987

Scambos T, Fricker H A, Liu C C, et al. 2009. Ice shelf disintegration by plate bending and hydro-fracture: Satellite observations and model results of the 2008 Wilkins ice shelf break-ups. Earth Planet Sci Lett, 1-4: 51–60

Scambos T, Haran T, Fahnestock M, et al. 2007. MODIS-based Mosaic of Antarctica (MOA) data sets: Continent-wide surface morphology and snow grain size. Remote Sens Environ, 2-3: 242–257

Scambos T, Hulbe C, Fahnestock M. 2003. Climate-induced ice shelf disintegration in the Antarctic Peninsula. Antarct Res Ser, 79: 79–92

Shuman C, Zwally H, Schutz B, et al. 2006. ICESat Antarctic elevation data: Preliminary precision and accuracy assessment. Geophys Res Lett, 7: L07501

Taurisano A, Tronstad S, Brandt O, et al. 2006. On the use of ground penetrating radar for detecting and reducing crevasse-hazard in Dronning Maud Land, Antarctica. Cold Reg Sci Technol, 3: 166–177

Van der Veen C. 1999. Crevasses on glaciers. Polar Geography, 3: 213–245

Vaughan D G. 1993. Relating the occurrence of crevasses to surface strain rates. J Glaciol, 132: 255–266
Vornberger P, Whillans I. 1990. Crevasse deformation and examples from Ice Stream B, Antarctica. J Glaciol, 122: 3–10
Wang X, Cheng X, Gong P, et al. 2011. Earth science applications of ICESat/GLAS: A review. Int J Remote Sens, 23: 8837–8864
Wang X, Cheng X, Li Z, et al. 2012. Lake water footprint identification from time-series ICESat/GLAS data. IEEE Geosci Remote Sensing, 3: 333–337
Weertman J. 1973. Can a water-filled crevasse reach the bottom surface of a glacier. IASH Publ, 95: 139–145
Xu T, Yang W, Liu Y, et al. 2011. Crevasse detection in Antarctica using ASTER images. In: Kamel M, Campilho A, eds. Image Analysis and Recognition. Heidelberg/Berlin: Springer. 370–379
Young N W, Hyland G. 2002. Velocity and strain rates derived from InSAR analysis over the Amery Ice Shelf, East Antarctica. Ann Glaciol, 1: 228–234
Zamora R, Casassa G, Rivera A, et al. 2007. Crevasse detection in glaciers of southern Chile and Antarctica by means of ground penetrating radar. IAHS Publications-Series of Proceedings and Reports, 318: 152–162
Zwally H, Schutz B, Abdalati W, et al. 2002. ICESat's laser measurements of polar ice, atmosphere, ocean, and land. J Geodyn, 3: 405–445